Mechatronics 42 (2017) 81–95

Contents lists available at ScienceDirect

Mechatronics

journal homepage: www.elsevier.com/locate/mechatronics

Design and validation of clutch-to-clutch shift actuator using dual-wedge mechanism

Li Chen[a,b,*], Fengyu Liu[b], Jian Yao[c], Zhao Ding[b], Chunhao Lee[c], Chi-kuan Kao[c], Farzad Samie[c], Ying Huang[c], Chengliang Yin[b]

[a] State Key Laboratory of Ocean Engineering, Collaborative Innovation Center for Advanced Ship and Deep-Sea Exploration, Shanghai Jiao Tong University, Shanghai 200240, PR China
[b] National Lab of Automotive Electronics and Control, Shanghai Jiao Tong University, Shanghai 200240, China
[c] General Motors

ARTICLE INFO

Article history:
Received 12 March 2016
Revised 17 January 2017
Accepted 21 January 2017

Keywords:
Clutch actuator
Clutch-to-clutch gearshift
Dual-wedge
Self-reinforced
Self-weakened

ABSTRACT

Clutch-to-clutch shift technology is a key enabler for fast and smooth gearshift for multi gear transmissions. However, conventional hydraulic actuation systems for clutches have drawbacks of oil leakage and low efficiency. Electromechanical devices including wedge mechanism offer potential alternative actuators. The previous studies on the wedge emphasize on self-reinforcement, but neglect self-weakened phenomenon. In this paper, a novel dual-wedge mechanism is proposed to exert self-reinforcement and avoid self-weakened effect by selecting a correct working slope. The design concept and physical structure are thoroughly described. Dynamic models for the actuation system and vehicle powertrain are built for performance validation. The results show that the normal force generated by the wedge under self-reinforced case is 2.74 times that under self-weakened case. Using the same amount of the driving motor current, the upshift can be successfully completed in 0.78 s when the correct slope is used; however, it fails to engage the clutch when the incorrect slope is used due to self-weakened effect. So does the downshift. Moreover, the experimental results of the dual-wedge mechanism using the correct slope are comparable to those from the hydraulic actuator of a conventional automatic transmission.

© 2017 Elsevier Ltd. All rights reserved.

1. Introduction

Taking advantage of continuous torque transmitting, clutch-to-clutch shift is more and more widely applied in modern vehicle transmissions, such as hydraulic automatic transmissions (AT) [1,2], dual clutch transmissions (DCT) [3,4] and the emerging electric variable transmissions (EVT) in hybrid electric vehicles [5,6]. The clutch-to-clutch shift leads seamless output torque by disengaging the off-going clutch simultaneously as engaging the on-coming clutch. The operations are manipulated by two actuators of the two clutches, respectively. Since the transmission efficiency is one of the significant factors of the vehicle efficiency, power consumption of the clutch actuators should be small in order to meet the requirement of the vehicle fuel economy.

Various technologies have been studied to reduce the power consumption of the clutch actuators. For example, an electric oil pump controlled by duty cycles is proposed to replace the engine-driven hydraulic pump which is always working [7] in the conventional hydraulic actuation systems. To avoid viscous friction losses and troublesome oil leakage, electromechanical devices are considered as potential high efficiency alternative actuators [8-10]. However, in order to provide sufficient engagement force in the clutch, the actuator mounted with a DCT in the small to mid-size sedans have the rated output usually between 150 and 300 W for a single clutch [11]. Thus, a large amount of electric energy is consumed, which adversely affects the overall vehicle efficiency.

Wedge mechanism, featuring self-reinforcement by making use of the friction force generated on one surface of the wedge, offers a power-saving concept of electromechanical clutch actuators [12,13,14]. Power-saving means the merits of less energy consumption, small size, less current of the driving motor and less joule loss. Motions of the wedge mechanism have been studied since decades before [15,16]. The initial investigation of a wedge brake was described in [17]. The comparison with the conventional braking system showed the average energy consumption of the eBrake actuator was reduced, and the actuator was downsized [12,18]. Optimization of the wedge brake is ongoing, such as removing backlash [19], cutting extra components [18], downsizing [20], improving control performance [21] and etc.. Similar to brakes, clutches

* Corresponding author.
E-mail address: li.h.chen@sjtu.edu.cn (L. Chen).

http://dx.doi.org/10.1016/j.mechatronics.2017.01.004
0957-4158/© 2017 Elsevier Ltd. All rights reserved.

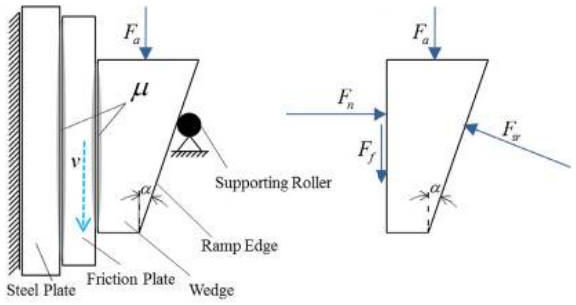

(a) Structure (b) Force analysis

Fig. 1. Principle of the wedge-based clutch actuation.

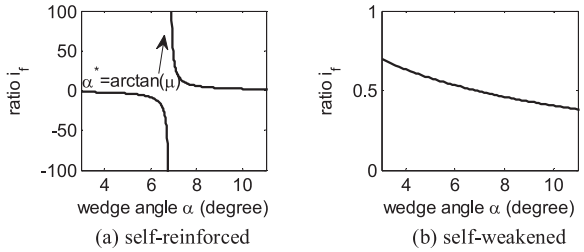

Fig. 2. Relationship between self-reinforcement ratio and wedge angle.

also have friction interfaces and control the vehicle longitudinal dynamics through friction torques. So the wedge mechanism was extended to the application of clutch actuations. A clutch actuator using rack and pinion as wedge mechanism was designed for the dry clutch of DCTs [11] and automated manual transmissions (AMTs) [13].

Other than the self-reinforced feature, the self-weakened effect of a wedge-actuated braking system was noticed [22]. Unfortunately, the previous designs have only one wedge slope, which cannot avoid self-weakened effect when the slipping speed on the friction interface is negative or the direction of the friction torque is negative. In MT or AMT, the slipping speed is negative when the engine speed is slower than the clutch output shaft speed, and the friction torque is negative when the engine is dragged by the vehicle inertia under engine braking case. In AT which consists of several planetary gear sets, negative slipping speed always occurs during clutch-to-clutch shift. So new mechanism is required to deal with the self-weakened problem. In our previous work [14], the static self-reinforcement characteristic of a wedge-based mechanism is analyzed for an AT. However, the self-weakened phenomena is omitted and the performance of clutch-to-clutch shift is not studied.

The contribution of this paper lies in two points: (1) realize the self-weakened phenomena of the wedge mechanism and design a new dual-wedge mechanism with two wedge slopes which can overcome the shortcoming of the self-weakened effect of previous wedge-based solutions; (2) analysis and test the performance of the motor-driven dual-wedge mechanism for the clutch-to-clutch shifts.

In this paper, the new design of the dual-wedge clutch actuator is described elaborately in Section 2. Following that, in Section 3, the dynamic model of the actuator is built, and a powertrain model is also deducted for system analysis. Section 4 gives the clutch-to-clutch shift control method for the motor-driven dual-wedge actuator, especially including the slope selection rule. In Section 5, simulation results are illustrated for both upshift and downshift cases using correct or incorrect selection of the two slopes; experimental results are also provided for the validation. Conclusions are drawn in Section 6.

2. Design of the dual-wedge mechanism

2.1. Design concept

The principle how a wedge mechanism is applied to a clutch is shown in Fig. 1(a). Generally, a clutch has two counterpart elements, i.e., the steel plate and the friction plate. They contact each other through friction surfaces. In terms of the number of the rotating elements, the clutches are classified into two types, i.e., braking clutch with one rotating element, and rotating clutch with two rotating elements. This study is focusing on the application of the braking clutch, in which the steel plate is considered as a static element.

The wedge is a trapezoid block featured by an angle α and a roller supporting the slope edge. The friction coefficient between the friction plate and long edge surface of the wedge is defined to be μ. The actuation force F_a is acting on the short edge surface of the wedge block.

Assuming the clutch slipping speed v is downward, denoted by $v > 0$, as shown in Fig. 1, the direction of the friction force F_f is also downward, and its magnitude is calculated as:

$$F_f = \mu F_n \tag{1}$$

in which, F_n is the normal force on the friction interface.

The force equilibrium equations of the wedge are:

$$F_a + F_f - F_{sr}\sin\alpha = 0 \tag{2}$$

$$F_n - F_{sr}\cos\alpha = 0 \tag{3}$$

in which, F_{sr} is the force passively generated on the supporting roller.

The amplification ratios i_f are obtained from (1), (2) and (3), respectively.

$$i_f = \frac{F_f}{F_a} = \frac{\mu}{\tan\alpha - \mu} \quad \text{when } v > 0 \tag{4}$$

As illustrated in Fig. 2(a), the ratio i_f varies along two individual curves with an increasing α for a given μ =0.12. The two curves are separated by a critical wedge angle $\alpha^* = \arctan(\mu)$. The left curve of the ratio i_f is negative because $\alpha < \arctan(\mu)$, whereas that of the right curve is positive because $\alpha > \arctan(\mu)$. For either of the two curves, the magnitude of i_f increases rapidly and mathematically approaches infinity when α approaches $\arctan(\mu)$. The big magnitude of i_f explains the self-reinforcement effect of the wedge mechanism. The sign of i_f means the direction of F_a, i.e., a positive i_f means the direction of F_a is the same as that of F_f, whereas a negative i_f means the direction of F_a is opposite to that of F_f. The latter brings more challenges for the actuation force control, therefore, α is always selected to make a positive i_f, i.e., $\alpha > \arctan(\mu)$.

Another assumption is that the clutch slip speed v in Fig. 1(a) changes to be upward, denoted by $v < 0$. Accordingly, the direction of F_f changes to be upward. Hence, the sign of F_f in (2) is replaced by a minus sign. Resultantly, the ratio i_f is calculated as:

$$i_f = \frac{F_f}{F_a} = -\frac{\mu}{\tan\alpha + \mu} \quad \text{when } v < 0 \tag{5}$$

It is obvious that the magnitude of i_f is less than 1 as shown in Fig. 2(b), so the actuation force is weakened in this case, which should be avoided in the design of a wedge-based actuator.

2.2. Physical structure

In this study, in order to ensure the self-reinforced effect and avoid the self-weakened effect no matter if the clutch slipping

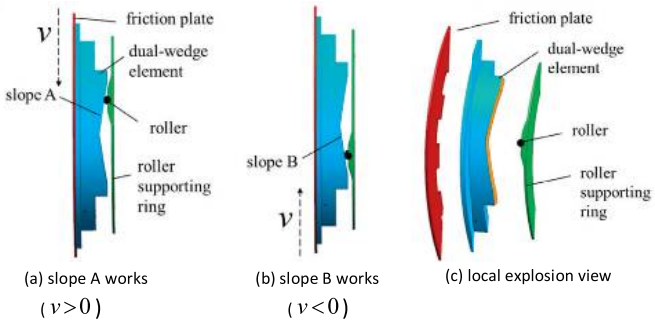

Fig. 3. Wedge element with two face to face slopes.

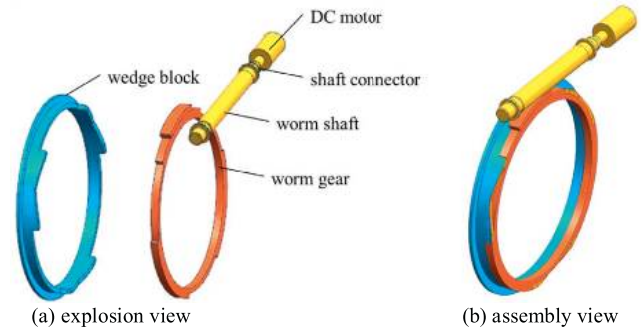

Fig. 4. Motor driven components.

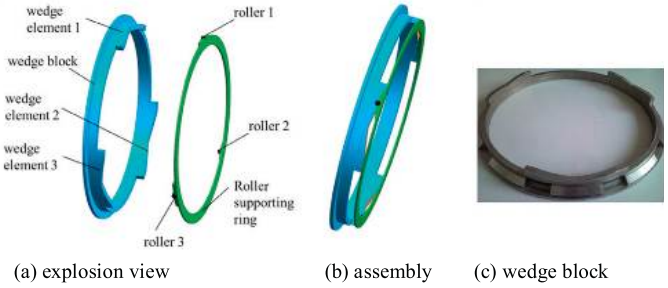

Fig. 5. Slopes on the wedge block.

speed is positive or negative, a dual-wedge element is designed with two face to face slopes (Slope A and Slope B), as shown in Fig. 3. According to (4) and (5), the selection of the two slopes depends on the sign of the clutch slipping speed v. If $v > 0$, slope A is selected to work, otherwise, if $v < 0$, slope B is selected.

The motion of the wedge block is driven by a motor, connected by a worm gear, worm shaft and shaft connector, as shown in Fig. 4. It is worth mentioning that the driving motor is parallel to the friction surface because of the wedge geometry, instead of being vertical. The parallel arrangement can make better use of space along the radial direction and occupy less space along the axial direction of a transmission. This arrangement is helpful for the transmission layout considering the axial space is always tight.

For the consideration of force distribution on the friction plate, three identical dual-wedge elements are circumferentially arranged every 120° in the wedge block, so do the rollers, as shown in Fig. 5.

For the convenience of test and validation, the proposed dual-wedge actuator is designed to fit a conventional AT. The hydraulic actuation system of one clutch is replaced by the new actuation. The transmission case is not changed; the friction plates (P5), steel plates (P4), wave plates (P13), return spring (P9) and retainer ring (P8) are reused. The wave plate acts as a cushion at the kiss point. The return spring is compressed to a certain position during engagement, and is released to push the hydraulic piston backward during disengagement. One end of the return spring is fixed by the retainer ring.

For the modified clutch, new components inside the transmission case include a wedge block (P7), a roller supporting ring (P11),three rollers (P10) and a worm gear (P6); and those outside the transmission case include a worm shaft (P3), a shaft connector (P2) and a DC motor (P1). The actuator is assembled into a modified six speed AT produced by General Motors. The assembling view and explosion view of the 3D model are given in Fig. 6(a) and (b), respectively. The actuator prototype is manufactured and installed in the AT, presented as the photo in Fig. 6(c).

2.3. Operation principle

First of all, before clutch engagement, the correct slope should be determined depending on the clutch slipping speed v. The motor current I_m is the control input of the motor-driven dual-wedge actuator, the angular displacement θ_m of the motor is the output of the actuator control, which physically corresponds to the axial displacement of the clutch plate and thereafter corresponds to the normal force on the friction plate. Taking Slope A as an example, the operation process during the clutch engagement and disengagement are described in the following paragraphs referring to Fig. 7.

During clutch engagement, the DC motor (P1) is operated by a certain amount of current. The output torque of the motor is transmitted to the worm gear (P6) through the mesh with worm shaft (P3). The worm gear (P6) is occlusive with the wedge block (P7) at the short edge surfaces. Thus, the force generated on the short edge surface drives the wedge block (P7) to move. The wedge block moves in two directions, i.e., moving along and rotating around the central axis. The two motions are constrained by the fixed roller (P10). The wedge block first moves to fill the clearance, and then generates self-reinforced friction force on the interface between the friction plate (P5) and the wedge block (P7). At the same time, the wave plate (P13) and return spring (P9) is compressed. As a result, the clutch slipping speed decreases gradually till the clutch comes to be locked at the end. Thus, the engagement process is completed.

During clutch disengagement, the motion of the components reverses. The normal force on the friction interface decreases so that the clutch starts to slip. When the wave plate (P13) completely releases, the normal force on the friction interfaces becomes zero. Then, the return spring (P9) releases, and the clutch comes back open with a clearance. Usually, the motor continues to pull the wedge block backward a bit more to ensure enough clearance for less parasitic loss. Thus, the disengagement process is completed.

3. Dynamic modeling

To validate the effectiveness of the actuator, two layers of dynamic model are discussed in this section, as shown in Fig. 8. The first layer is the actuator model, including the DC motor and the mechanical components from the shaft connector to the wedge block and clutch plates. The second layer is the clutch-to-clutch shift involved driveline model, including the engine, torque converter, planetary gearbox and vehicle. The models of the second layer are described in Appendix.

The schematic of the actuator is shown in side view and top view in Fig. 9. First of all, the wedge block is modeled followed by the DC motor, worm shaft, worm gear and clutch plate. These objects are modeled as rigid bodies, ignoring their stiffness and damping effect. Nevertheless, the stiffness and damping effect of

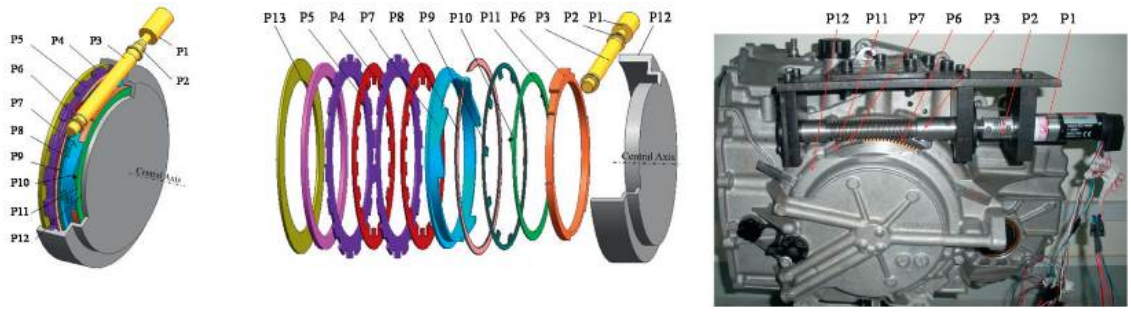

a) assembly view (b) explosion view (c) prototype

P1	DC motor	P2	shaft connector	P3	worm shaft	P4	steel plates	P5	friction plates
P6	worm gear	P7	wedge block	P8	retainer ring	P9	return spring	P10	roller
P11	supporting Ring	P12	transmission case	P13	wave plate				

Fig. 6. 3D model and prototype of the dual-wedge clutch actuator.

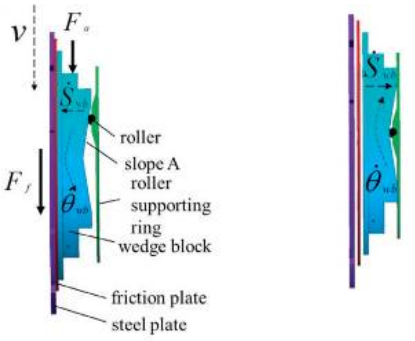

(a) Engagement (b)Disengagement

Fig. 7. Operation principle of the dual-wedge clutch actuator.

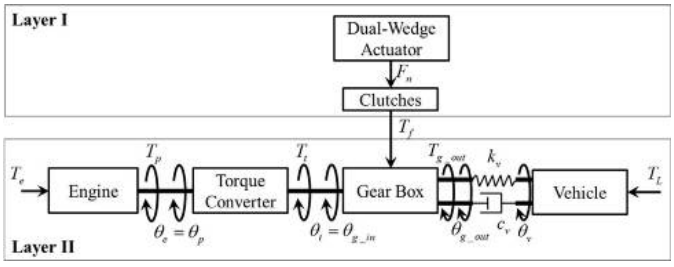

Fig. 8. Diagram of dynamic model.

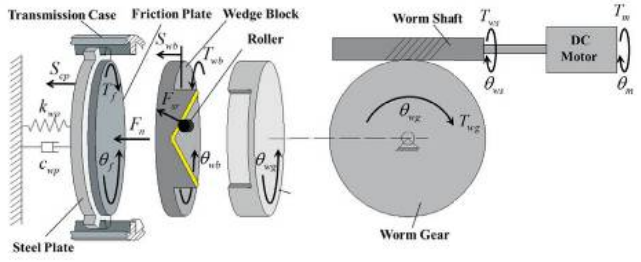

(a) Side view (b) Top view

Fig. 9. Schematic of the dual-wedge clutch actuator.

the spring pack (wave plate and return spring) is considered. After that, a set of summarized equation is derived in terms of the contact status of the friction interface.

3.1. Wedge block

The three wedge elements on the wedge block are simplified as one element since their motions are identical. The motion of the wedge block along the axis is described as:

$$m_{wb}\ddot{S}_{wb} = F_{sr}\cos\alpha - F_n \tag{6}$$

in which, m_{wb} and S_{wb} denote the mass and axial displacement of the wedge block, respectively.

The rotation of the wedge block around the axis is described as

$$J_{wb}\ddot{\theta}_{wb} = T_{wb} + T_f - WF_{sr}R_{wb}\sin\alpha \tag{7}$$

in which, J_{wb}, θ_{wb}, R_{wb}, T_{wb} and T_f denote the moment of inertia, angular displacement, radius, driving torque and friction torque of the wedge block, respectively. The slope factor W is defined as:

$$\begin{aligned} W &= 1 \quad \text{when Slope A works} \\ W &= -1 \quad \text{when Slope B works} \end{aligned} \tag{8}$$

Since the wedge block moves against the supporting roller, the translational and rotational movements are subject to the constraint:

$$S_{wb} = W\theta_{wb}R_{wb}\tan\alpha \tag{9}$$

Therefore, by substituting S_{wb} by the above expression, the dynamic Eqs. (6) and (7) is derived as:

$$(J_{wb} + m_{wb}R_{wb}^2\tan\alpha^2)\ddot{\theta}_{wb} = T_{wb} + T_f - WF_n\tan\alpha R_{wb} \tag{10}$$

3.2. DC motor

The dynamics of the DC motor is described as follows [23]:

$$J_m\ddot{\theta}_m = T_m - T_{ws} \tag{11}$$

$$T_m = K_t I_m \tag{12}$$

in which, J_m, θ_m, T_m, K_t, I_m denote the moment of inertia, angular displacement, output torque, torque constant, current of the motor, respectively. The reaction torque from the worm shaft is denoted by T_{ws}.

3.3. Worm shaft and worm gear

The dynamic equations are written as:

$$J_{ws}\ddot{\theta}_{ws} = T_{ws} - T_{wg}/n \tag{13}$$

$$J_{wg}\ddot{\theta}_{wg} = T_{wg} - T_{wb} \tag{14}$$

in which, J_{ws} and J_{wg} are the moment of inertia of the worm shaft and worm gear, respectively. The angular displacements of the worm shaft and worm gear are denoted by θ_{ws} and θ_{wg}, respectively. The reaction torque from the worm gear is denoted by T_{wg}.

The speed ratio n of the worm shaft over the worm gear is:

$$n = \dot{\theta}_{ws}/\dot{\theta}_{wg} \tag{15}$$

Because the shaft connector between the worm shaft and the DC motor is considered as rigid, there exists:

$$\theta_{ws} = \theta_m \tag{16}$$

Similarly, because the worm gear is splined with the wedge block, there exists:

$$\theta_{wg} = \theta_{wb} \tag{17}$$

3.4. Clutch plate

The clutch plate has two degrees of freedom of motion, i.e., moving along and rotating around the central axis. The moving dynamics is determined by the actuator, and the rotating dynamics is determined by the connected driveline. The former is discussed in this section, and the latter will be discussed in next section. Apart from those, the relationship between the normal force F_n and the friction torque T_f is covered by the clutch plate model, and is presented in this section.

The moving dynamics along the axis of the clutch plate is written as:

$$m_{cp}\ddot{S}_{cp} = F_n - k_{wp}S_{cp} - c_{wp}\dot{S}_{cp} \tag{18}$$

in which, m_{cp} and S_{cp} denote the moment of inertia and axial displacement of the clutch plate, respectively; k_{wp} and c_{wp} denote the stiffness and damping coefficient of the spring pack, respectively.

By defining S_{wb0} to be the clearance between the friction plate and wedge block when the clutch is open, there exists:

$$\begin{aligned} &F_n = 0,\ S_{cp} = 0 \quad \text{when } S_{wb} < S_{wb0} \\ &S_{cp} = S_{wb} - S_{wb0} \quad \text{when } S_{wb} \geq S_{wb0} \end{aligned} \tag{19}$$

The friction torque T_f is calculated by:

$$T_f = \mu N R_{cp} F_n \tag{20}$$

in which, N is the number of friction interfaces of the clutch, and R_{cp} is the equivalent radius of the clutch friction interface.

For computation convenience, the friction coefficient μ is smoothened as below [24] instead of using the discontinuous Coulomb model:

$$\mu(\omega) = \left[1.0 + \left(\frac{\mu_s}{\mu_k} - 1.0\right) e^{-\varsigma \cdot abs(\omega)}\right] \cdot \tanh\left(\xi \cdot \omega \cdot R_{cp}\right) \tag{21}$$

in which, μ_s and μ_k denote the slipping friction and static friction coefficient, respectively; ς and ξ are two tuning parameters.

On the friction interface between the friction plate and the steel plate, the slipping speed ω is defined by:

$$\omega = \dot{\theta}_f \tag{22}$$

where, $\dot{\theta}_f$ is the angular velocity of the friction plate.

On the friction interface between the friction plate and the wedge block, the slipping speed ω is defined by:

$$\omega = \dot{\theta}_f - \dot{\theta}_{wb} \tag{23}$$

where $\dot{\theta}_{wb}$ is calculated by (10).

3.5. Complete model equations

The summarization is given in terms of the contact status of the dual-wedge clutch. When the wedge block contacts the frictional plate, the governing equations include six independent differential Eqs.((6), (7), (11), (13), (14) and (18)) with six motion constraints((9), (15), (16), (17) and (19)). The unknown variables include six state variables (S_{wb},θ_{wb},θ_m,θ_{ws}, θ_{wg}, S_{cp}) and six forces(F_{sr}, F_n, T_f, T_{wb}, T_{ws}, T_{wg}). Therefore, the sum of the equation number and the constraint number equals to the sum of the unknown variables. Theoretically, these equations can have deterministic solution.

The resultant equation is:

$$\begin{aligned} J\ddot{\theta}_{wb} = {} & nT_m + T_f - k_{wp}R_{cp}^2\tan^2\alpha\theta_{wb} - c_{wp}R_{cp}^2\tan^2\alpha\dot{\theta}_{wb} \\ & + k_{wp}R_{cp}^2\tan^2\alpha\theta_{wb0} \end{aligned} \tag{24}$$

in which, the moment of inertia J is calculated as:

$$J = J_{wg} + n^2 J_{ws} + n^2 J_m + J_{wb} + m_{wb} R_{wb}^2 \tan^2\alpha + m_{cp} R_{cp}^2 \tan^2\alpha \tag{25}$$

When the wedge block does not contact with the frictional plate, i.e., the clutch is open, the governing equation can be simplified from (24) with $T_f = 0$ as:

$$J_o\ddot{\theta}_{wb} = nT_m \tag{26}$$

in which

$$J_o = J_{wg} + n^2 J_{ws} + n^2 J_m + J_{wb} + m_{wb} R_{wb}^2 \tan^2\alpha \tag{27}$$

It can be seen that a uniform expression is obtained for both Slope A and Slope B in (24) and (26). Nevertheless, the dynamics is nonlinear due to the nonlinearity of the friction torque T_f with respect to the clutch slipping speed ω as expressed in (21). According to the wedge principle analyzed in Section II, the dual-wedge actuation system behaves self-reinforced effect when the direction of T_f is the same as that of the motor torque T_m, otherwise, the system behaves self-weakened effect.

4. Clutch-to-Clutch shift control method

The dual-wedge actuator is designed with the target of being comparable to the conventional hydraulic actuation system of the clutch-to-clutch shift, whose typical application is the AT. The clutch-to-clutch shift process of the AT is controlled by adjusting the piston fluid pressure of the oncoming clutch and the offgoing clutch, respectively. The normal force F_n is proportional to the piston fluid pressure once the friction plates touch the steel plates. The desired F_n of the dual-wedge clutch actuator is the same as that of the conventional AT, however, is realized by the new actuator.

In order to track the desired normal force F_n precisely, the motor current profiles are calibrated carefully based on the information of the angular displacement θ_m of the motor, considering that an open loop control cannot guarantee the accuracy due to the dynamics and hysteresis of the actuator components. In the experiments that the motor moves at constant speed, the motor current differs over 20% between the two opposite directions. So the position feedback with dedicated clutch inverse transfer function cannot achieve precise tracking. Owing to the motion constraints expressed in (9), (15)–(17) and (19), the displacement θ_m corresponds to the displacement S_{cp} of the clutch plate which is the closest component to the friction interface, regardless of the dynamics and hysteresis. Moreover, the dynamic Eq. (18) defines the relationship between the normal force F_n and the displacement S_{cp}; therefore, the desired S_{cp} can be calculated given the desired F_n; thereafter, the desired θ_m can be obtained. On the other hand, the major portion of F_n comes from the large stiffness k_{wp} of the

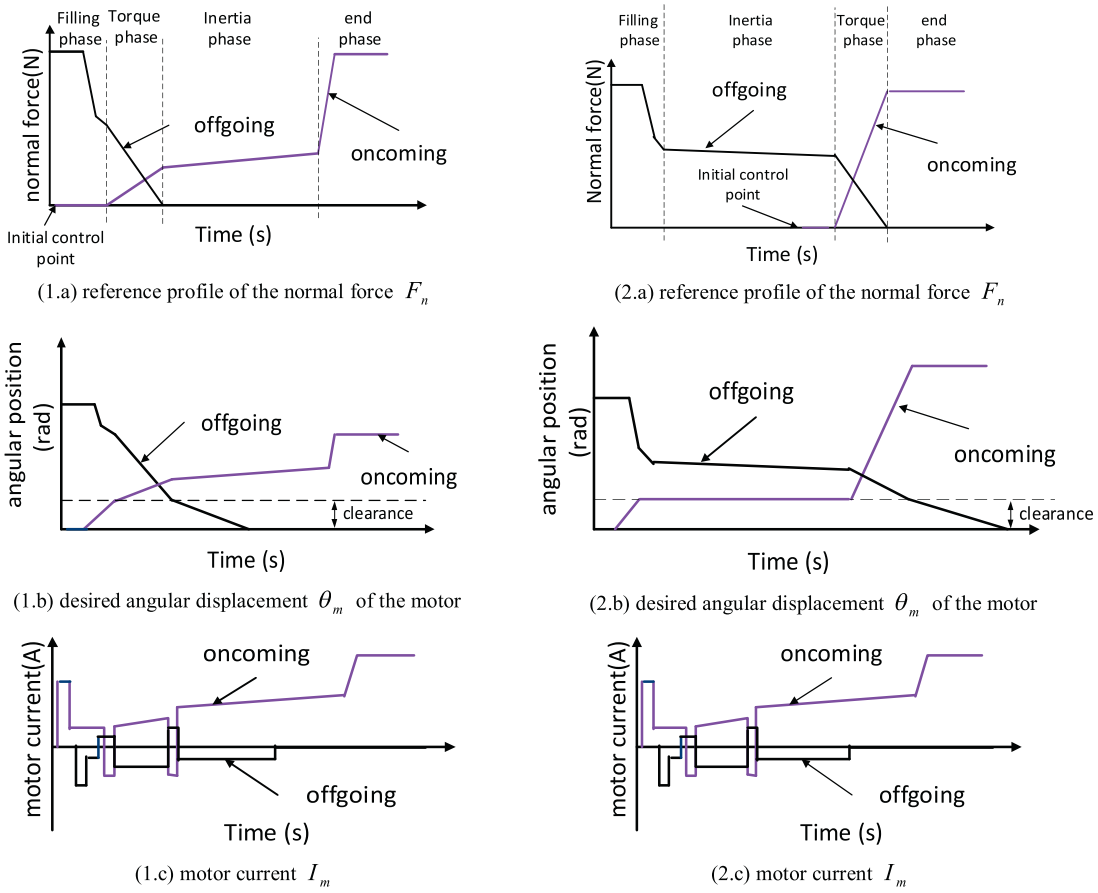

Fig. 10. Clutch-to-clutch shift control process (1.a–1.c) upshift; (2.a–2.c) downshift.

spring pack because the motions $\dot{S}_{cp}$ and $\ddot{S}_{cp}$ are rather small when the friction plate contacts the steel plate as seen from (18), therefore the calculation of the desired θ_m can be simplified by the ignorance of the two terms.

With the purpose of validating the advantage of the proposed actuator, this study refers to the normal force profiles of the conventional AT, and carefully calibrates the controller to track the desired normal force. A generic clutch-to-clutch upshift consists of four phases in sequence, i.e., filling phase, torque phase, inertia phase and end phase [27,28], as shown in Fig. 10(1.a). In the filling phase, the actuation system fills the clearance of the oncoming clutch and is ready for clutch normal force regulation. At the same time, the normal force of the offgoing clutch is reduced to slowly ramp down in the next stage. In the torque phase, the drive torque is transferred from the offgoing clutch to the oncoming clutch by the increasing the normal force of the oncoming clutch and decreasing that of the offgoing clutch accordingly. By the end of the torque phase, the torque ratio of the transmission has been changed to the ratio associated with the target gear, and all the drive torque is carried by the oncoming clutch. In the inertia phase, the offgoing clutch is open, and the normal force of the oncoming clutch is calibrated using the speed information to complete the change of the speed ratio. In the end phase, the normal force of the oncoming clutch is commanded to the maximum possible value to lock the clutch.

The reference profile of the normal force F_n is adopted from [29] and [30], as shown in Fig. 10(1.a) and (2.a). The desired angular displacement θ_m of the motor is shown in Fig. 10(1.b) and (2.b). The qualitative sketches plotted in Fig. 10(1.c) and (2.c) offer the instruction of the calibration, but they are not the numerical results. The numerical results are provided in the next sections on simulation and experiments. The calibration rules are described in the following paragraphs in terms of upshift and downshift, respectively.

4.1. Upshift control

In order to achieve the reference normal force F_n, the motor currents I_m are calibrated to track the desired angular displacement θ_m of the motor as shown in Fig. 10 (1.b). The calibration rules are described as below.

(1) In the filling phase, first of all, a correct wedge slope should be selected for the oncoming clutch according to the slipping speed ω of the friction interface. If $\omega > 0$, Slope A is selected; otherwise, if $\omega < 0$, Slope B is selected. Taking Slope A as an example, the motor of the oncoming clutch applies a large positive current I_m, then a small I_m followed by a negative I_m. In this way, the motor starts up at the beginning, then rotates at a moderate speed to pass through the clearance, and then decelerates to a slow speed at the end of the filling phase. Thus, the motor overcomes the clearance without rushing into the next phase. As to the offgoing clutch, its motor firstly applies a large negative I_m, then a small negative I_m followed by a positive I_m. In this way, the motor angular displacement θ_m decreases at a large reverse rotating speed, then continues to decrease at a medium speed, and then at a slow speed being ready for torque transferring. If Slope B is selected, the sign of the motor current I_m is opposite to the above, though, the magnitude is the same as

the above. Due to the page limitation, the following rules are described taking Slope A as the example.

(2) In the torque phase, the motor of the oncoming clutch applies a large positive I_m followed by a negative I_m. In this way, the motor angular displacement θ_m increases at a large speed, then continues at a slow speed at the end of the torque phase. As to the offgoing clutch, its motor applies a large negative I_m followed by a small positive I_m. The motor angular displacement θ_m decreases at a large reverse rotating speed, then continues to decrease at a slow speed.

(3) In the inertia phase, the motor of the oncoming clutch applies moderately increasing I_m. In this way, the motor angular displacement θ_m increases gradually. As to the offgoing clutch, its motor applies a negative I_m. The motor angular displacement θ_m decreases until the clutch has enough clearance for the purpose of less spin loss.

(4) In the end phase, the motor of the oncoming clutch applies the largest I_m. Thus, the motor angular displacement θ_m reaches the maximum value and the normal force F_n also reaches the maximum value.

4.2. Downshift control

Different from the upshift process, the downshift process implements the inertia phase before the torque phase. The reason is that, the engine speed needs to be lifted up to avoid being towed since the engine speed is less than the output shaft speed of the oncoming clutch before the down shift starts. In order to achieve the reference normal force F_n, the motor currents I_m are calibrated to track the desired angular displacement θ_m of the motor as shown in Fig. 10 (2.a). The processes of the filling phase and end phase are similar to those of the upshift, so their description is omitted so as to avoid redundancy.

(1) In the inertia phase, the motor current I_m of the oncoming clutch is zero. So the motor angular displacement θ_m does not change, and the oncoming clutch is just waiting for the start of the torque phase. The motor of the offgoing clutch applies a moderate negative I_m. In this way, the motor angular displacement θ_m decreases so as to decrease the normal force F_n on the offgoing clutch. Thus, the offgoing clutch slips and the oncoming clutch can be synchronized by the aiding of the engine speed control.

(2) In the torque phase, the motor of the oncoming clutch applies a large positive I_m. In this way, the motor angular displacement θ_m increases to its maximum end and the normal force F_n also increases to the maximum value. As to the offgoing clutch, its motor applies a large negative I_m followed by a small negative I_m. The motor angular displacement θ_m decreases quickly at first and then gradually until there is enough clearance.

5. Simulation results

The gear shift process can take advantage of the self-reinforcement when a correct slope of the dual-wedge block is selected for the engagement of the oncoming clutch. On the other hand, self-weakened effect occurs when an incorrect slope is selected. This section starts with the comparison between self-reinforced and self-weakened effect in the same upshift operation. After that, the results of two self-reinforced cases are illustrated, one is a downshift process using Slope A, and the other is an upshift process using Slope B. In addition, the results from the conventional hydraulic actuation of the AT using the models we have already developed are also provided for convenient comparison of the shift performance. The parameters used in the simulation are given in Tables 1 and 2.

Table 1
Parameters of the dual-wedge actuator.

c_{wp}	100 N•s/m	R_{cp}	0.105 m
J_m	0.0004 kg•m^2	R_{wb}	0.1 m
J_{wb}	0.0082 kg•m^2	S_{wb0}	0.002 m
J_{wg}	0.0036 kg•m^2	α	10°
J_{ws}	0.0030 kg•m^2	ς	6
k_{wp}	1.3×10^6 Nm/m	ξ	100
m_{cp}	0.75 kg	μ_s	0.14
m_{wb}	0.87 kg	μ_k	0.12
n	164		

Table 2
Parameters of the powertrain.

A_v	2 m^2	J_v	11.3 kg•m2
c_{air}	0.3	k_v	15,000 Nm/rad
c_v	150 Nm•s/rad	m_v	1705 kg
g	9.81 m/s^2	R_{tr}	0.314 m
i_d	3.87	ρ	1.2 kg/m^3
J_e	0.137 kg•m^2	μ_R	0.015

5.1. Comparison between the self-reinforced and self-weakened effect

During the upshift process from the 1st to 2nd gear of the six-speed AT as shown in Fig. A.3, the oncoming clutch CB26 is to be engaged, and the offgoing clutch CB1R is to be disengaged. The upshift process is operated in a moderate acceleration pedal which generates the engine throttle opening $\alpha_{th} = 50\%$. Because the clutch slipping speed $\dot{\theta}_f$ of the oncoming clutch is positive as shown in Fig. 11(1.f), the correct slope for self-reinforcement is Slope A according to the rule given in Section 4. Similarly, the offgoing clutch also uses its Slope A. For comparison, the results of Slope B, which leads to self-weakened effect, are also provided in Fig. 11.

By using Slope A, the upshift process starts from 3.09 s, and completes in 0.78 s. The normal force on the oncoming clutch increases gradually in the filling and torque phase, keeps moderately flat in the inertia phase, and increases rapidly from 1508 N to 3314 N in 0.12 s in the end phase, as shown in Fig. 11(1.e). This profile is approximately identical to that of the conventional hydraulic actuation as shown in Fig. 11(3.b), which is obtained by hydraulic pressure regulation in Fig. 11(3.a). Thereafter, the clutch slipping speed in Fig. 11(1.f) and the output torque in Fig. 10(1.g) are approximately identical to those of the conventional hydraulic actuation in Fig. 11(3.c and 3.d). In addition, these results are comparable to those in the literatures [28,31].

It can be seen from Fig. 11(1.a) that the motor current I_m frequently changes to regulate the normal force. The capability of the motor control is critical for the clutch-to-clutch shift performance, just like that the capability of the hydraulic system control is critical for the shift performance of the conventional AT. In general, the response from the motor current I_m to the motor toque T_m is as fast as an instant according to the principle of electromagnetics, there is great potential for the motor to satisfy the requirement of the clutch-to-clutch shift control. Moreover, the motor control takes the angular displacement θ_m of the motor as the output signal as shown in Fig. 11(1.b). The calibration based on the angular displacement θ_m can be effective in dealing with the influence of the dynamics and hysteresis of the actuation components.

By using Slope B, the oncoming clutch engagement fails as seen in Fig. 11(2.f). It is noticed that the amount of motor current as shown in Fig. 11(2.a) is the same as that using Slope A but in opposite sign of operation, however, the normal force generated on the oncoming clutch as shown in Fig. 11(2.e) is much less than that using Slope A. Consequently, the output torque T_v using Slope

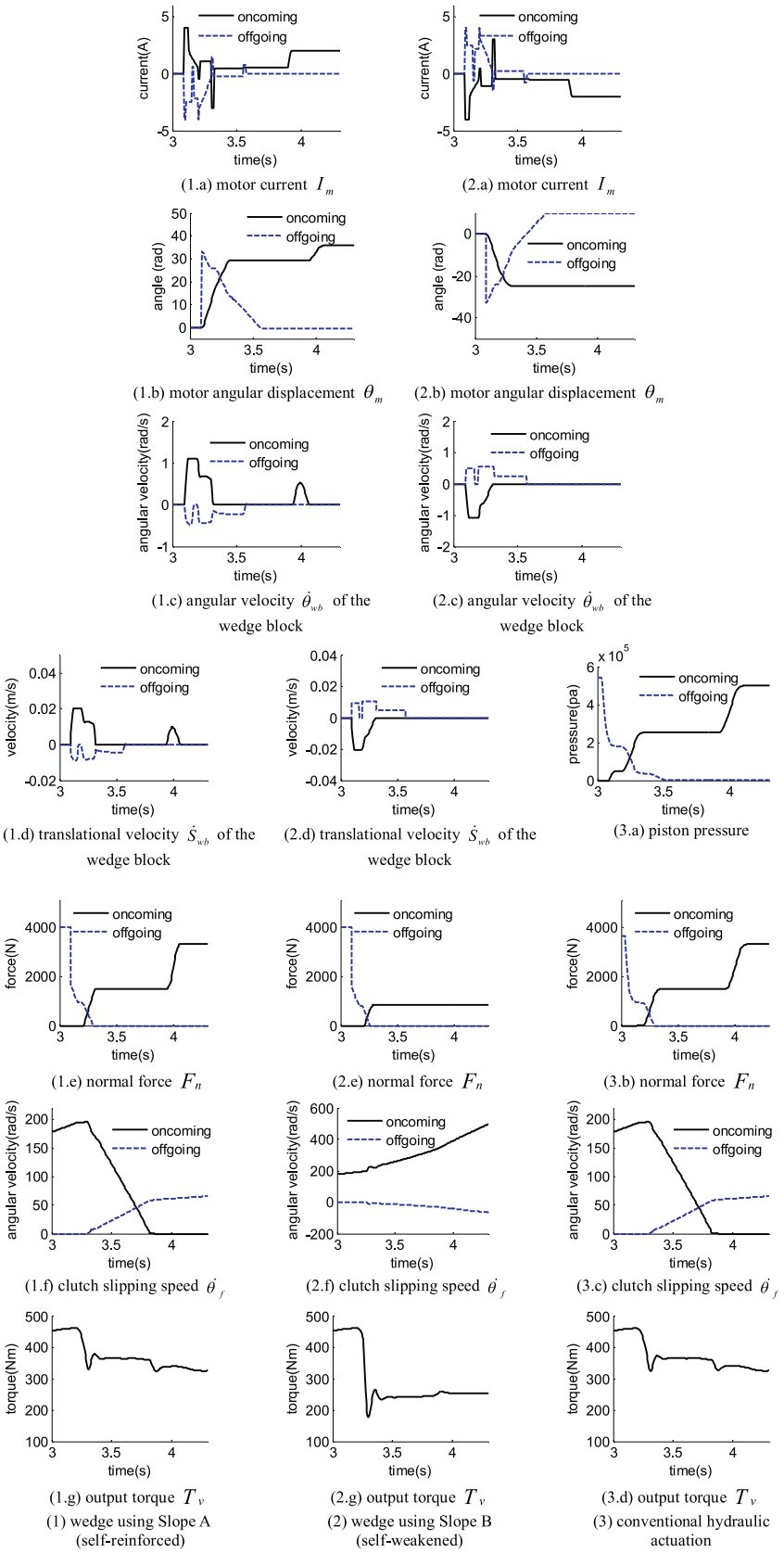

(1.a) motor current I_m (2.a) motor current I_m

(1.b) motor angular displacement θ_m (2.b) motor angular displacement θ_m

(1.c) angular velocity $\dot{\theta}_{wb}$ of the wedge block (2.c) angular velocity $\dot{\theta}_{wb}$ of the wedge block

(1.d) translational velocity $\dot{S}_{wb}$ of the wedge block (2.d) translational velocity $\dot{S}_{wb}$ of the wedge block (3.a) piston pressure

(1.e) normal force F_n (2.e) normal force F_n (3.b) normal force F_n

(1.f) clutch slipping speed $\dot{\theta}_f$ (2.f) clutch slipping speed $\dot{\theta}_f$ (3.c) clutch slipping speed $\dot{\theta}_f$

(1.g) output torque T_v (2.g) output torque T_v (3.d) output torque T_v

(1) wedge using Slope A (self-reinforced) (2) wedge using Slope B (self-weakened) (3) conventional hydraulic actuation

Fig. 11. Comparison of the self-reinforced wedge, self-weakened wedge and conventional hydraulic actuation during upshift.

B is about half of that using Slope A, as shown in Fig. 11(2.g). The clutch cannot complete the shift and carry the full input torque, resultantly, the slipping speed of the oncoming clutch keeps increasing and can never be closed.

Similar differences between the results of self-reinforced and self-weakened effect are found in other cases. Due to page limitation, the results of self-weakened effect are not presented in the following two cases.

5.2. Self-reinforced by Slope A during a downshift

As shown in Fig. 12, the downshift process from 2nd to 1st gear successfully completes in 0.81 s. Because the clutch slipping speed $\dot{\theta}_f$ of the oncoming clutch is positive as shown in Fig. 12(1.f), the correct slope for self-reinforcement is Slope A. So, the wedge block, driven by the motor with a positive current I_m, rotates with a positive rotary speed $\dot{\theta}_{wb}$ and moves ahead with a positive translational speed $\dot{S}_{wb}$, as shown in Fig. 12(1.a), (1.c) and (1.d).

The maximum motor current I_m is 4A as shown in Fig. 12(1.a). The angular displacement of the motor θ_m is shown in Fig. 12(1.b), which is rather similar to the profile of the normal force F_n in Fig. 12(1.e). The normal force of the oncoming clutch can be up to 4350 N, and increases promptly from zero to 4350 N in 0.08 s. The normal force generated by the wedge based actuation is almost identical to that by the hydraulic system as shown in Fig. 12(3.b), which is obtained by hydraulic pressure regulation as shown in Fig. 12(3.a).

The output torque is obviously decreased in the inertia phase because the desired output torque is zero at zero throttle opening. Other than this fluctuation, no peak is found in the output torque profile, so the shift quality is acceptable. As a whole, the shift performance is comparable to that of the conventional hydraulic system as illustrated in Fig. 12(2.c) and (2.d).

5.3. Self-reinforced by Slope B during an Upshift

Because of the planetary gear set configuration, the initial clutch slipping speed $\dot{\theta}_f$ is negative as shown in Fig. 13(1.f) during the upshift from the 5th to 6th gear. Therefore, Slope B is selected for self-reinforcement purpose. Thus, the wedge block is driven by a negative motor current, rotates in negative direction, as shown in Fig. 13(1.a) and (1.c), and move ahead as shown in Fig. 13(1.d).

The upshift process successfully completes in 1.0 s. The maximum motor current I_m is 4A as shown in Fig. 13(1.a). The angular displacement of the motor θ_m is shown in Fig. 13(1.b), which is rather similar to the profile of the normal force F_n in Fig. 13(1.e). In the end phase, the normal force F_n of the oncoming clutch increases rapidly from 842 N to 4853 N in 0.12 s. The output torque as shown in Fig. 13(1.g), which is similar to that of the conventional hydraulic system in Fig. 13(3.d). The output torque fluctuates in a flat style, which means the shift quality is acceptable.

6. Experimental results

The prototype in Fig. 6 is fabricated with one of the clutches (CB26) in the AT modified and actuated by the proposed dual-wedge mechanism. The mature AT is selected as the benchmark of the dual-wedge actuation because the AT has typical clutch components. It is expected that the proposed design can achieve comparable performance to the mature hydraulic clutch actuation of the AT. The comparison does not mean the replacement of the hydraulic system of the AT because the hydraulic system may be the most suitable actuation for the AT due to the advantage of the flexible connection between the pump and more than four sets of clutches. However, the application of the proposed design can be

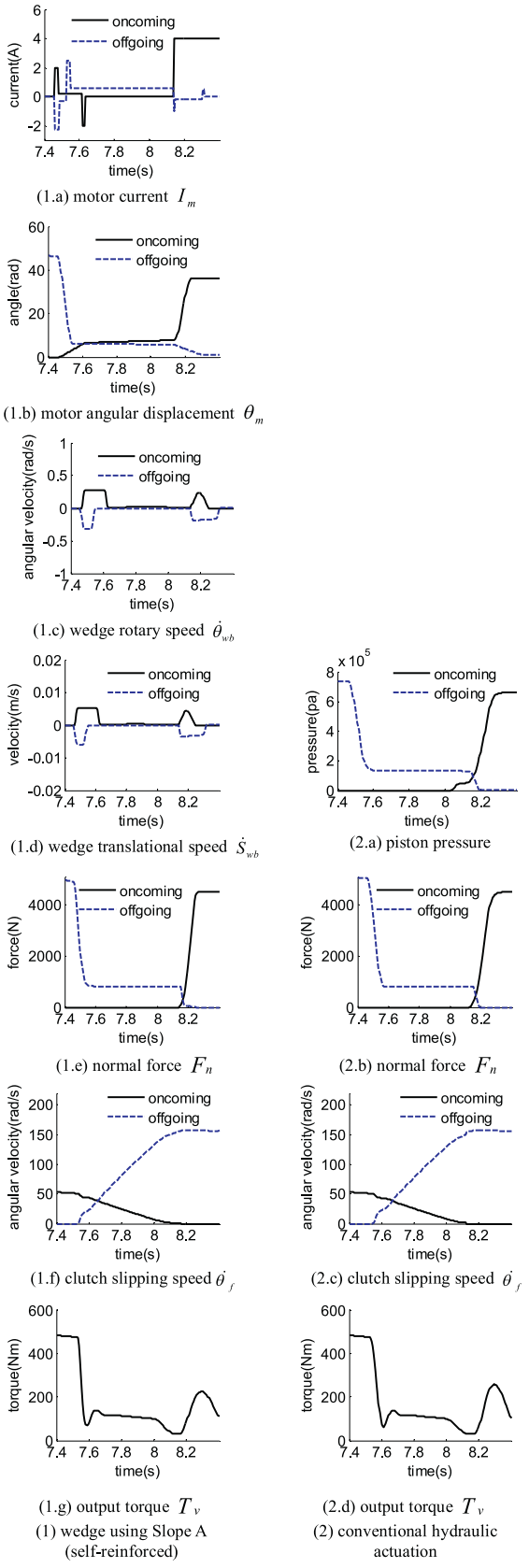

Fig. 12.. Comparison of the dual-wedge (self-reinforced using Slope A) and conventional hydraulic actuation during downshift.

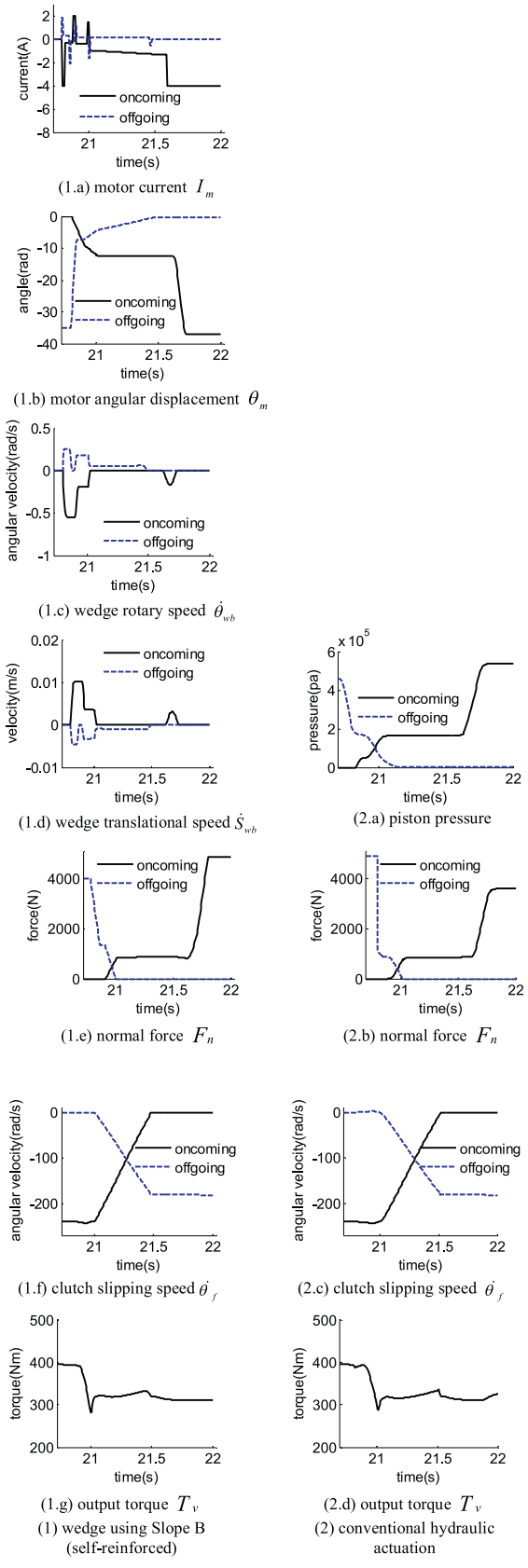

Fig. 13. Comparison of the dual-wedge (self-reinforced using Slope B) and conventional hydraulic actuation during upshift.

expanded to other clutch relevant areas. The experiments are implemented on a set of dynamometer depicted in Fig. 14. The input dynamometer is to emulate the engine transient with rated torque 297 Nm and maximum speed 6500 rpm. The load dynamometer is to emulate the vehicle driving resistance with rated torque 486 Nm and maximum speed 5000 rpm. A set of flywheel, placed before the load dynamometer, is used to emulate the moment of inertia of the vehicle. The six speed AT is arranged between the input dynamometer and the flywheel.

Three force sensors are deployed on the plates of the clutch CB26 to measure the normal force on the clutch plates. The force range is up to 2000 N for each sensor. Apart from those, two torque sensors (A and B), with rated measurement range of 500Nm and 3000Nm, are used to measure the input torque and load torque of the AT, respectively. Two encoders (A and B) are used to measure the input speed and output speed of the AT.

Referring to the two layers of the dynamic model, the experiments are implemented in two steps. The first step is to study the characteristic of the motor-driven dual-wedge clutch actuator, i.e., self-reinforced or self-weakened in terms of the two slopes. The second step is to check the clutch-to-clutch shift quality relying on the dual-wedge actuation system.

In the experiment, the AT is during the upshift process from the 1st to 2nd gear, i.e., the oncoming clutch CB26 is to be engaged, and the offgoing clutch CB1R is to be disengaged.

6.1. Characteristics of the dual-wedge clutch actuator

The input dynamometer is working in speed mode to maintain 100 rpm (in positive direction) for the rotating part of CB26. In this experiment, it is unnecessary to apply load to the AT, so the load dynamometer and the flywheel is not connected to the output shaft of the AT. According to the wedge mechanism principle, self-reinforced effect occurs when Slope A is selected to work by a positive motor current I_m; otherwise, self-weakened effect occurs when Slope B is selected to work by a negative motor current I_m, despite with the same amount. The current profile is operated to emulate those during gearshift as in (a) of Fig. 11–13.

The comparison between the self-reinforced and self-weakened effect is given in Fig. 15. The simulation results are provided together with the experimental results. The legend “exp.” is the short name of “experiment”, and “sim.” is “simulation” .

The major differences between the self-reinforced and self-weakened case lie in two aspects. First of all, as seen from Fig. 15(d), the normal force F_n under the self-reinforced case is 2.74 times that under the self-weakened case, which validates the significance of the slope selection for the purpose of self-reinforcement.

The second aspect is on the motion direction of the wedge. It is interesting that the wedge translational speed $\dot{S}_{wb}$ is positive for both the two cases, i.e., self-reinforced case with positive motor current I_m and self-weakened case with positive motor current I_m, as shown in Fig. 15(a) and (c). This phenomena comes from the dual-wedge structure as shown in Fig. 3, and most importantly, this structure ensures the wedge block can be pushed ahead to engage the clutch no matter the wedge is rotating in positive or reverse direction.

6.2. Clutch-to-clutch shift experiment

In the experiment, the oncoming clutch CB26 is actuated by the proposed wedge prototype, while offgoing clutch C1R is still actuated by the original hydraulic piston (As seen from the simulation results, the oncoming clutch plays a major significant role in shift quality). So the dual-wedge actuator has to cooperate with the mature hydraulic actuation system to complete a clutch-to-clutch

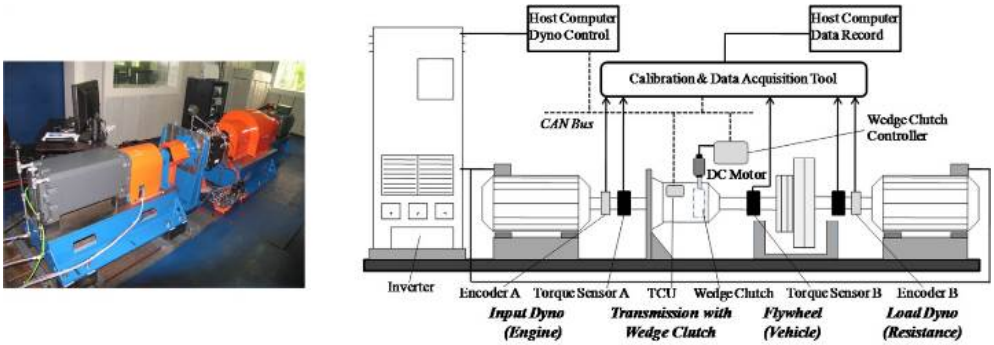

Fig. 14.. Layout of the dynamometer facilities.

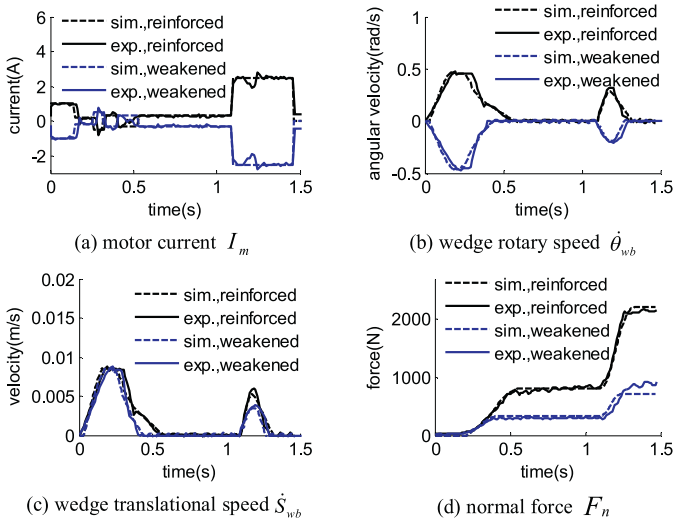

Fig. 15.. Characteristics of the dual-wedge clutch actuator.

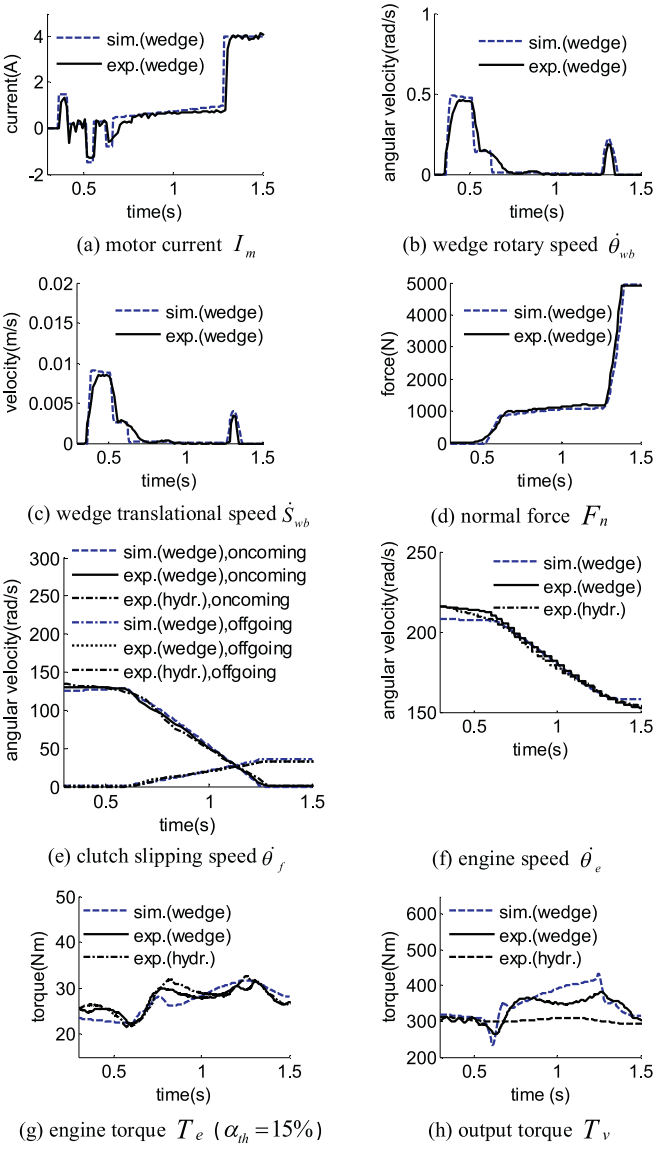

Fig. 16.. Clutch-to-clutch shift experiment (1st to 2nd gear).

gearshift process. The input dynamometer is working in torque mode to emulate the output torque T_e as in Fig. A.1 of an engine at throttle opening $\alpha_{th} = 15\%$. The flywheel is connected to the output shaft of the AT, and the output dynamometer is also working in torque mode to emulate the load torque T_L as in (A.22) of a vehicle. The initial speed of the flywheel is zero. The gear set is initially at the 1st gear by configuring the conventional TCU (transmission control unit). The control of CB26 of the TCU is bypassed by a controller developed for the dual-wedge actuator. The results from the dynamometer experiment and simulation are compared in Fig. 16. Besides, the experimental results of the conventional hydraulic actuation are also provided for comparison.

Because the clutch slipping speed $\dot{\theta}_f$ of the clutch CB26 is positive at the beginning of the gearshift, Slope A is selected; resultantly, the wedge rotary speed $\dot{\theta}_{wb}$ is positive, so does the wedge translational speed$\dot{S}_{wb}$, as shown in Fig. 16(a)–(c).

As seen from Fig. 16(e), the upshift process actuated by the dual-wedge mechanism successfully completes in 1.04 s. The maximum motor current is 4A as seen in Fig. 16(a), and the normal force generated on the friction plate is up to 5000 N. Moreover, the normal force increases from zero to 5000 N in as short as 0.14 s in the end phase. This profile shows that the normal force can be controlled elaborately and satisfy the requirement of clutch-to-clutch gearshift. No intensive jerk is found in the output torque profile as Fig. 16(f), nevertheless, fluctuation occurs with a peak in the end of the inertia phase. By the comparison between Fig. 16(g) and (h), the fluctuation before the peak reflects the change of the engine torque. At the peak moment, the motor current increases instantly and the normal force increases rapidly. This increasing induces stick-slip transition dynamics of the clutch friction plate. More refined calibration and insight dynamics need to be studied further.

The comparison between the dual-wedge actuation and the conventional hydraulic actuation can be seen in Figure 16(e)-(h). As a whole, the simulation results from the dual-wedge clutch match the experimental results well. Moreover, the results from the dual-wedge clutch actuator are comparable to those from the conventional hydraulic actuator.

7. Conclusions

A motor-driven dual-wedge clutch actuation system is proposed for clutch-to-clutch gear shift. The dual-wedge mechanism can exert self-reinforced effect and avoid self-weakened effect by selecting a correct wedge slope for either positive or negative slipping speed of the clutch. The new mechanism is applied to the clutch-to-clutch gearshift of an AT.

The experimental results validate the normal force generated by the wedge under self-reinforced case is 2.74 times that under self-weakened case. Under the same amount of driving motor current, the gearshift from 1st to 2nd gear can be successfully completed in 0.78 s when Slope A is used for self-reinforcement effect; however, it fails to engage the clutch when Slope B is used due to self-weakened effect. Similarly, under self-reinforcement case, the downshift from 2nd to 1st gear is completed in 0.81 s using Slope A, and the upshift from 5th to 6th gear is completed in 1.0 s using Slope B.

Moreover, the experimental results of the dual-wedge mechanism are comparable to those from the conventional hydraulic actuator of the AT. Therefore, the application of the proposed dual-wedge mechanism to other transmissions, such as DCT, AMT and EVT, is worthy of further study.

Acknowledgement

The authors would like to thank the National Natural Science Foundation of China for the supports on this project (Grant no. 51475284).

Appendix

The dynamic model of the powertrain is described as below.

(1) Engine

The dynamic equation is described as below, with an engine map $T_e(\dot{\theta}_e, \alpha_{th})$ as shown in Fig. A.1.

$$J_e\ddot{\theta}_e = T_e(\dot{\theta}_e, \alpha_{th}) - T_p \tag{A.1}$$

where J_e, θ_e, α_{th} and T_e are the moment of inertia, angular displacement, throttle opening and output torque of the engine; T_p is the reaction torque from the pump of the torque converter.

(2) Torque converter

A torque convertor has a pump as a torque input element, and a turbine as a torque output element. The pump torque T_p and turbine torque T_t are calculated as:

$$T_p = C(\lambda)\dot{\theta}_p^2 \tag{A.2}$$

$$T_t = t(\lambda)T_p \tag{A.3}$$

in which, θ_p is the angular displacement of the pump, and the ratio λ is defined as:

$$\lambda = \dot{\theta}_t/\dot{\theta}_p \tag{A.4}$$

The capacity factor $C(\lambda)$ and the torque ratio $t(\lambda)$ are given in Fig. A.2.

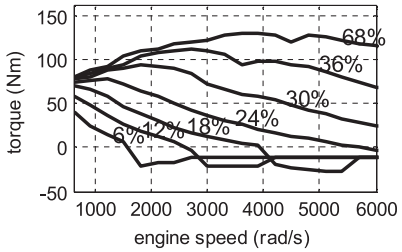

Fig. A.1. Engine map $T_e = f(\dot{\theta}_e, \alpha_{th})$.

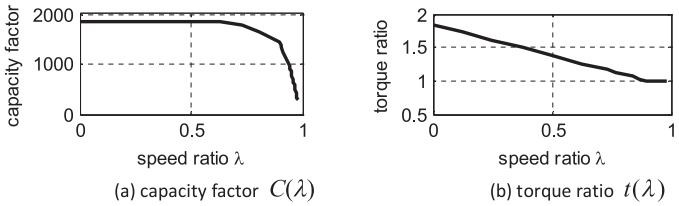

Fig. A.2. Parameters of the torque converter.

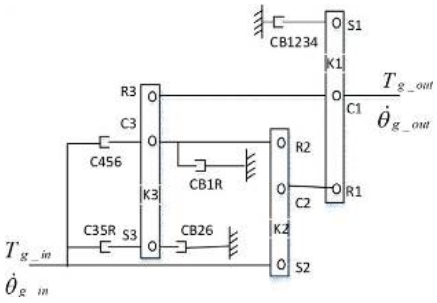

Fig. A.3. Lever diagram of the six-speed AT.

Since the torque convertor connects the engine and the gear box, there exists:

$$\dot{\theta}_p = \dot{\theta}_e \tag{A.5}$$

$$\dot{\theta}_t = \dot{\theta}_{g\_in} \tag{A.6}$$

where θ_{g_in} is the angular displacement of the input shaft of the gear box.

(3) Gearbox

A six-speed AT with three planetary gear sets as shown in Fig. A.3 is modeled by using the Lever analogy method [25]. Three braking clutches (C1234, CB1R and CB26) and two rotating clutches (C456 and C35R) are employed. At any of the six gear ratios, two of the five clutches are locked. Theoretically, the three planetary gear sets have six motion DOFs (degrees of freedom), however, they are constrained by three fixed connections (from R3 to C1, from C3 to R2, from C2 to R1) and two locked clutches. Resultantly, only one motion DOF remains, which means the velocities of all the elements are determined by the input velocity $\dot{\theta}_{g\_in}$, and the torques are determined by the input torque T_{g_in}. The variables to be obtained include: the output velocity$\dot{\theta}_{g_out}$, the velocities of the two locked clutches (denoted by$\dot{\theta}_{lc_1}$ and $\dot{\theta}_{lc\_2}$), the output torque T_{g_out}, and the transmitted torques of the two locked clutches(T_{lc_1} and T_{lc_2}). There exists torque transformation matrix $A$and velocity transformation matrix B as below, respectively. The expressions of A and B are related to the parameters and connection topology of the planetary gear box.

The three planetary gearsets in Fig. A.3 are represented with subscript 1, 2 and 3, respectively. Each gearset includes a ring gear, a sun gear and a carrier, represented by R, S and C, respectively.

Let K denote the ratio of the ring gear over the sun gear of the planetary gearset.

The torque equilibrium equations of the three gearsets are described as:

$$\begin{aligned} &T_{C3}+(K_3+1)\,T_{S3}=0\\ &T_{C2}+(K_2+1)\,T_{S2}=0\\ &T_{C1}+(K_1+1)\,T_{S1}=0 \end{aligned} \tag{A.7}$$

Taking the first gear with locked CB1R (denoted with the subscript lc_1) and CB1234(denoted with the subscript lc_2) as an example, the torques are subject to the following 6 constraints:

$$\begin{aligned} &T_{S3}\cdot K_3+T_{C1}-T_{out}=0\\ &T_{S2}-T_{in}=0\\ &T_{C3}+T_{S2}\cdot K_2+T_{lc\_1}=0\\ &T_{S3}=0\\ &T_{S1}\cdot K_1+T_{C2}=0\\ &T_{S1}+T_{lc\_2}=0 \end{aligned} \tag{A.8}$$

It can be seen from (A.7) and (A.8) that the ten torque variables are subject to the nine equations. Therefore, only one torque variable is independent. Defining T_{g_in} to be the independent variable, the transformation matrix can be deducted from (A.7) and (A.8) as below.

$$\begin{aligned} &[T_{C1}\quad T_{S1}\quad T_{C2}\quad T_{S2}\quad T_{C3}\quad T_{S3}\quad T_{lc\_1}\quad T_{lc\_2}\quad T_{g\_out}]^T\\ &=A_p^T[T_{g\_in}] \end{aligned} \tag{A.9}$$

in which, A_p is a 8×1 matrix calculated by:

$$A_p=\begin{bmatrix} 0 & 0 & 0 & 0 & 1 & (K_3+1) & 0 & 0 & 0\\ 0 & 0 & 1 & (K_2+1) & 0 & 0 & 0 & 0 & 0\\ 1 & (K_1+1) & 0 & 0 & 0 & 0 & 0 & 0 & 0\\ 1 & 0 & 0 & 0 & 0 & K_3 & 0 & 0 & -1\\ 0 & 0 & 0 & 1 & 0 & 0 & 0 & 0 & 0\\ 0 & 0 & 0 & K_2 & 1 & 0 & 1 & 0 & 0\\ 0 & 0 & 0 & 0 & 0 & 1 & 0 & 0 & 0\\ 0 & K_1 & 1 & 0 & 0 & 0 & 0 & 0 & 0\\ 0 & 1 & 0 & 0 & 0 & 0 & 0 & 1 & 0 \end{bmatrix}^{-1} \cdot \begin{bmatrix} 0\\0\\0\\0\\1\\0\\0\\0\\0 \end{bmatrix} \tag{A.10}$$

Therefore, the matrix A can be selected from A_p so as to satisfy the equation as below.

$$\begin{bmatrix} T_{lc\_1}\\ T_{lc\_2}\\ T_{g\_out} \end{bmatrix}=A\left[T_{g\_in}\right] \tag{A.11}$$

in which,

$$A=[A_p(7,1)\quad A_p(8,1)\quad A_p(9,1)]^T \tag{A.12}$$

The kinematic constraints of the three gearsets are described as below.

$$\begin{aligned} &K_3\,\dot\theta_{R3}-\dot\theta_{S3}-(K_3-1)\,\dot\theta_{C3}=0\\ &K_2\,\dot\theta_{R2}-\dot\theta_{S2}-(K_2-1)\,\dot\theta_{C2}=0\\ &K_1\,\dot\theta_{R1}-\dot\theta_{S1}-(K_1-1)\,\dot\theta_{C1}=0 \end{aligned} \tag{A.13}$$

The connection topology of the three gearsets complies with the following 9 kinematic constraints.

$$\begin{aligned} &\dot\theta_{S1}=0\\ &\dot\theta_{R3}=\dot\theta_{C1}\\ &\dot\theta_{C3}=\dot\theta_{R2}\\ &\dot\theta_{C2}=\dot\theta_{R1}\\ &\dot\theta_{R2}=0\\ &\dot\theta_{lc\_1}=\dot\theta_{S1}\\ &\dot\theta_{lc\_2}=\dot\theta_{R2}\\ &\dot\theta_{g\_in}=\dot\theta_{S2}\\ &\dot\theta_{g\_out}=\dot\theta_{C1} \end{aligned} \tag{A.14}$$

It can be seen that the 12 state variables in (A.13) and (A.14) are subject to the 11 constraint equations. Therefore, only one state variable is independent. Defining $\dot\theta_{g\_in}$ to be the independent variable, the transformation matrix can be deducted from (A.13) and (A.14) as below.

$$\begin{aligned} &[\dot\theta_{R3}\quad \dot\theta_{C3}\quad \dot\theta_{S3}\quad \dot\theta_{lc\_2}\quad \dot\theta_{C2}\quad \dot\theta_{R1}\quad \dot\theta_{g\_out}\quad \dot\theta_{lc\_1}]^T\\ &=B_p\cdot[\dot\theta_{g\_in}] \end{aligned} \tag{A.15}$$

in which, B_p is a 8×1 matrix calculated by:

$$B_p=\begin{bmatrix} K_3 & -(K_3-1) & -1 & 0 & 0 & 0 & 0 & 0\\ 0 & 0 & 0 & K_2 & -(K_2-1) & 0 & 0 & 0\\ 0 & 0 & 0 & 0 & 0 & K_1 & -(K_1-1) & -1\\ 0 & 0 & 0 & 0 & 0 & 0 & 0 & 1\\ 1 & 0 & 0 & 0 & 0 & 0 & -1 & 0\\ 0 & 1 & 0 & -1 & 0 & 0 & 0 & 0\\ 0 & 0 & 0 & 0 & 1 & -1 & 0 & 0\\ 0 & 0 & 0 & 1 & 0 & 0 & 0 & 0 \end{bmatrix}^{-1} \cdot \begin{bmatrix} 0\\-1\\0\\0\\0\\0\\0\\0 \end{bmatrix} \tag{A.16}$$

Therefore, the matrix B can be selected from B_p so as to satisfy the equation as below.

$$\begin{bmatrix} \dot\theta_{lc\_1}\\ \dot\theta_{lc\_2}\\ \dot\theta_{g\_out} \end{bmatrix}=B\left[\dot\theta_{g\_in}\right] \tag{A.17}$$

in which,

$$B=[B_p(8,1)\quad B_p(4,1)\quad B_p(7,1)]^T \tag{A.18}$$

During gearshift, the three gearsets have two motion degrees of freedom because one of the two locked clutches is released. During upshift from the 1st to 2nd gear, the clutch CB26 (denoted with the subscript f_1) is to be engaged(oncoming), and the clutch CB1R (denoted with the subscript f_2) is to be disen-

gaged(offgoing). The torque constraint equations are:

$$\begin{aligned} &T_{S3}\cdot K_3 + T_{C1} - T_{out} = 0\\ &T_{S2} - T_{in} = 0\\ &T_{C3} + T_{S2}\cdot K_2 + T_{f\_2} = 0\\ &T_{S3} + T_{f\_1} = 0\\ &T_{S1}\cdot K_1 + T_{C2} = 0 \end{aligned} \tag{A.19}$$

The 10 torque variables are subject to the 8 equations of (A.7) and (A.19). Therefore, there are 2 independent torque variables. Defining T_{f_1} and T_{f_2} to be the independent variables, the transformation matrix can be deducted from (A.7) and (A.19) as below.

$$[T_{C1}\quad T_{S1}\quad T_{C2}\quad T_{S2}\quad T_{C3}\quad T_{S3}\quad T_{g\_in}\quad T_{g\_out}]^T = C_p\cdot\begin{bmatrix} T_{f\_1}\\ T_{f\_2}\end{bmatrix} \tag{A.20}$$

in which, C_p is a 8 × 2 matrix calculated by:

$$C_p = \begin{bmatrix} 0 & 0 & 0 & 0 & 1 & (K_3+1) & 0 & 0\\ 0 & 0 & 1 & (K_2+1) & 0 & 0 & 0 & 0\\ 1 & (K_1+1) & 0 & 0 & 0 & 0 & 0 & 0\\ 1 & 0 & 0 & 0 & 0 & K_3 & 0 & -1\\ 0 & 0 & 0 & 1 & 0 & 0 & -1 & 0\\ 0 & 0 & 0 & K_2 & 1 & 0 & 0 & 0\\ 0 & 0 & 0 & 0 & 0 & 1 & 0 & 0\\ 0 & K_1 & 1 & 0 & 0 & 0 & 0 & 0 \end{bmatrix}^{-1} \cdot \begin{bmatrix} 0 & 0\\ 0 & 0\\ 0 & 0\\ 0 & 0\\ 0 & 0\\ 0 & -1\\ -1 & 0\\ 0 & 0 \end{bmatrix} \tag{A.21}$$

Therefore, the matrix C can be selected from C_p so as to satisfy the equation as below.

$$\begin{bmatrix} T_{g\_in}\\ T_{g\_out}\end{bmatrix} = C\begin{bmatrix} T_{f\_1}\\ T_{f\_2}\end{bmatrix} \tag{A.22}$$

in which,

$$C = \begin{bmatrix} C_p(7,1) & C_p(7,2)\\ C_p(8,1) & C_p(8,2)\end{bmatrix} \tag{A.23}$$

During the upshift from the 1st to 2nd gear, the connection topology yields the following kinematic constraint equations:

$$\begin{aligned} &\dot\theta_{R3} = \dot\theta_{C1}\\ &\dot\theta_{C3} = \dot\theta_{R2}\\ &\dot\theta_{C2} = \dot\theta_{R1}\\ &\dot\theta_{S1} = 0 \end{aligned} \tag{A.24}$$

It can be seen that the nine state variables in (A.13) and (A.24) are subject to the eight constraint equations. Therefore, there are two independent state variables. Defining $\dot\theta_{S2}$ and $\dot\theta_{C1}$ to be the independent variables, the transformation matrix can be deducted from (A.13) and (A.24) as below.

$$[\dot\theta_{R3}\quad \dot\theta_{C3}\quad \dot\theta_{S3}\quad \dot\theta_{R2}\quad \dot\theta_{C2}\quad \dot\theta_{R1}\quad \dot\theta_{S1}\quad]^T = D_p\begin{bmatrix}\dot\theta_{S2}\\ \dot\theta_{C1}\end{bmatrix} \tag{A.25}$$

in which, D_p is a 8 × 2 matrix calculated by:

$$D_p = \begin{bmatrix} K_3 & -(K_3-1) & -1 & 0 & 0 & 0 & 0\\ 0 & 0 & 0 & K_2 & -(K_2-1) & 0 & 0\\ 0 & 0 & 0 & 0 & 0 & K_1 & -1\\ 1 & 0 & 0 & 0 & 0 & 0 & 0\\ 0 & 1 & 0 & -1 & 0 & 0 & 0\\ 0 & 0 & 0 & 0 & 1 & -1 & 0\\ 0 & 0 & 0 & 0 & 0 & 0 & 1 \end{bmatrix}^T \cdot \begin{bmatrix} 0 & 0\\ 1 & 0\\ 0 & K_1-1\\ 0 & 1\\ 0 & 0\\ 0 & 0\\ 0 & 0 \end{bmatrix} \tag{A.26}$$

Therefore, the matrix D can be selected from D_p so as to satisfy the equation as below.

$$\begin{bmatrix}\dot\theta_{f\_1}\\ \dot\theta_{f\_2}\end{bmatrix} = D\begin{bmatrix}\dot\theta_{g\_in}\\ \dot\theta_{g\_out}\end{bmatrix} \tag{A.27}$$

in which,

$$D = \begin{bmatrix} D_p(3,1) & D_p(3,2)\\ D_p(4,1) & D_p(4,2)\end{bmatrix} \tag{A.28}$$

4) Vehicle

The dynamic equation is derived as

$$J_v\ddot\theta_v = k_v(\theta_{g\_out} - \theta_v) + c_v(\dot\theta_{g\_out} - \dot\theta_v) - T_L \tag{A.29}$$

where J_v, k_v, c_v and θ_v are the moment of inertia, stiffness, damping coefficient and angular displacement of equivalent shaft of the vehicle body; T_L is the load torque.

For the case that the vehicle is running on flat road, the load torque T_L consists of the frontal drag and rolling resistance, calculated by [26]:

$$T_L = \left(\frac{1}{2}\rho c_{air}A_v\left(\dot\theta_v\cdot\frac{R_{tr}}{i_d}\right)^2 + \mu_R m_v g\right)\cdot\frac{R_{tr}}{i_d} \tag{A.30}$$

where ρ and c_{air} are the air density, air damping coefficient respectively; A_v and $m_v$are the frontal surface area and mass of the vehicle, respectively; R_{tr} is the tire radius, i_d is the final drive gear ratio, and g stands for the gravity.

Therefore, the output torque T_v towing the vehicle can be calculated from (A.29) as:

$$T_v = k_v(\theta_{g\_out} - \theta_v) + c_v(\dot\theta_{g\_out} - \dot\theta_v) = J_v\ddot\theta_v + T_L \tag{A.31}$$

References

[1] You M, Wen Q, Zheng M, Li Z. The design of transmission scheme of the 6-speed automatic transmission based on the 01 N automatic transmission. *Adv Mater Res* 2013;605-607:1217–23.

[2] Lu X, Wang S, Liu Y, Xu X. Application of clutch to clutch gear shift technology for a new automatic transmission. *J Cent South Univ* 2012;19(10):2788–96.

[3] Berkel K, Hofman T, Serrarens A, Steinbuch M. Fast and smooth clutch engagement control for dual-clutch transmissions. *Control Eng Pract* 2014;22:57–68.

[4] Walker PD, Zhang N. Modelling of dual clutch transmission equipped powertrains for shift transient simulations. *Mech Mach Theory* 2013;60:47–59.

[5] Zhu F, Chen L, Yin C. Design and analysis of a novel multi-mode transmission for a HEV using a single electric machine. *IEEE Trans Veh Technol* 2013;62(3):1911–22.

[6] Ehsani M, Gao Y, Emadi A. Modern electric, hybrid electric, and fuel cell vehicles: fundamentals, theory, and design. CRC Press; 2009.

[7] Kim Y, Lee J, Jo C, et al. Development and Control of an Electric Oil Pump for Automatic Transmission-Based Hybrid Electric Vehicle. *Veh Technol IEEE Trans* 2011;60(5):1981–90.

[8] Liu H, Chen X, Cao P, Zhang Q. Modelling and analysis of a novel mechanism for EMT actuator. *Appl Mech Mater* 2013;321-324:46–50.

[9] Wagner U, Berger R, Ehrlich M, et al. Electromotoric actuators for double clutch transmissions 8th LuK symposium; 2006.

[10] J. Wheals, A. Turner, K. Ramsay, et al., "Double clutch transmission(dct) using multiplexed linear actuation technology and dry clutches for high efficiency and low cost," SAE 2007-01-1096.
[11] Oh JiwonJ, Kim Jinsung, Choi SeibumB. Design of self-energizing clutch actuator for dual-clutch transmission. Mechatron IEEE/ASME Trans APRIL 2016;21(2).
[12] Roberts R, Schaut M, Hartmann, H. Modelling and validation of the mechatronic wedge brake. *SAE Trans* 2003;112:2376–86.
[13] Kim J, Choi SB. Design and modeling of a clutch actuator system with self-energizing mechanism. *Mechatron IEEE/ASME Trans* 2011;16:953–66.
[14] Yao J, Chen L, Yin CL, et al. Modeling of a Wedge Clutch in an Automatic Transmission; 2010. SAE Paper p. 01–0186.
[15] Wick C. How gm uses wedge rolling. Manuf Eng 1977;78(2):33–4.
[16] Morozov AI. Wedge-shapd piezoelectric semiconductor transducer for ultrasonic surface waves. Sov Phys Semicond 1972;5(10):1732–3.
[17] Hartmann H, Schaut M, Pascucci A, et al. eBrake(R)-the Mechatronic Wedge Brake; 2002. SAE Paper p. 01–2582.
[18] Roberts RP, Gombert B, Hartmann H, et al. Testing the Mechatronic Wedge Brake; 2004. SAE Paper p. 01–2766.
[19] Fox J, Roberts R, Baier-Welt C, et al. Modeling and Control of a Single Motor Electronic Wedge Brake; 2007. SAE Paper p. 01–0866.
[20] Kim JG, Kim MJ, Kim JK. Developing of Electronic Wedge Brake with Cross Wedge; 2009. SAE Paper p. 01–0856.
[21] Jo CH, Song HL, Cho YS, et al. Design and control of an upper-wedge-type electronic brake. In: Proceedings of the institution of mechanical engineers, Part D: journal of automobile engineering, 224; 2010. p. 1393.
[22] Chen L, Xi G. Stability and response of a self-amplified braking system under velocity-dependent actuation force. Nonlinear Dyn 2014;78(4):2459–77.
[23] Rigatos GG. Adaptive fuzzy control of DC motors using state and output feedback. *Electr Power Syst Res* 2009;79:1579–92.
[24] Awrejcewicz J, Grzelczyk D, Pyryev Y. A novel dry friction modeling and its impact on differential equations computation and Lyapunov exponents estimation. J Vibroeng 2008;10(4):475–82.
[25] H.L. Benford, M.B. Leising. "The Lever Analogy: A New Tool in Transmission Analysis," SAE paper, No 810102.
[26] Fundamentals of Vehicle Dynamics, SAE International, 1992-02-15
[27] Meng F, Zhang H, Cao D, et al. System modeling, coupling analysis, and experimental validation of a proportional pressure valve with pulsewidth modulation control[J]. IEEE/ASME Trans Mechatron 2016;21(3):1742–53.
[28] S. Bai, R.L. Moses, T. Schanz, and M.J. Gorman, "Development of a New Clutch-to-Clutch Shift Control Technology," SAE Technical Paper 2002.
[29] Wentao S, Huiyan C. Research on control strategy of shifting progress; 2008. SAE, Warrendale, PA, USA, Tech. Paper no. 2008-01-1684.
[30] Meng F, Zhang H, Cao D, et al. System modeling and pressure control of a clutch actuator for heavy-duty automatic transmission systems[J]. IEEE Trans Veh Technol 2015 1-1.
[31] Gao B, Liu X, Chen H, Lu X, Li J. Dynamics and control of gear upshift in automated manual transmissions. Int. J. Vehicle Design 2013;63(1).